Dijet and electroweak limits on a Z' boson coupled to quarks

Bogdan A. Dobrescu[1] and Felix Yu[2]

[1]*Particle Theory Department, Fermilab, Batavia, Illinois 60510, USA*
[2]*PRISMA+ Cluster of Excellence and Mainz Institute for Theoretical Physics,
Johannes Gutenberg University, 55099 Mainz, Germany*

An insightful way of presenting the LHC limits on dijet resonances is the coupling-mass plot for a Z' boson that has flavor-independent quark interactions. This also illustrates the comparison of low-mass LHC sensitivity with constraints on the flavor-independent Z' boson from electroweak and quarkonium measurements. To derive these constraints, we compute the Z' mixing with the Z, the photon, and the Υ meson, emphasizing the logarithmic dependence on the masses of the new electroweak-charged fermions ("anomalons") required to cancel the gauge anomalies. We update the coupling-mass plot, extending it for Z' masses from 5 GeV to 5 TeV.

I. INTRODUCTION

In the past few years, significant efforts have proven successful at advancing hadron collider sensitivity to electroweak scale dijet resonances. At the end of run 1 of the Large Hadron Collider (LHC), in 2014, the ATLAS and CMS experiments had leading experimental sensitivity to $\mathcal{O}(\text{TeV})$ dijet resonances, but previous hadron collider experiments such as UA2 and CDF still provided the leading constraint for resonances below a few hundred GeV [1–4]. The situation has now changed, with the advent of advanced triggering techniques to overcome the intrinsic large quantum chromodynamic (QCD) background at low dijet masses as well as dedicated efforts to probe resonances in associated production modes [5–17]. These more specialized searches are complemented by the high-mass analyses [18–22], which have been impressively extended to dijet resonances as heavy as several TeV.

Searches for dijet resonances are powerful probes of many theories beyond the Standard Model (SM), because any particle produced in the s channel can decay back into two partons which then hadronize. In models with an additional $U(1)$ gauge symmetry, such as gauged baryon number [23–33], the phenomenology of the associated Z' boson is mainly characterized by two parameters, the Z' mass and its gauge coupling. Searches spanning different collider environments can then most easily be interpreted in the coupling-versus-mass plane [3], highlighting

opportunities for further collider searches to cover possible gaps in sensitivity.

Here, we reiterate that Z' models generically include additional new particles and analyze how parameters associated with those particles impact the Z' properties. The new particles include at least one scalar associated with the $U(1)$ symmetry-breaking sector and some fermions ("anomalons") charged under both the $U(1)$ and the SM gauge groups, required to cancel the gauge anomalies. Even when the Z' boson cannot decay into non-SM particles, its mixing with the SM spin-1 fields are impacted at one-loop level by the masses and couplings of the anomalons.

Nevertheless, the hadron collider limits are adequately captured by the gauge coupling versus Z' mass plot. Comparing the limits from hadron colliders with the electroweak data and other low-energy constraints, however, needs a detailed analysis. We perform this analysis and extend the coupling-versus-mass plot from 5 GeV to 5 TeV, with exemplary choices of the anomalon parameters controlling the mixing-induced constraints. It turns out that the dependence on those parameters affects only the low-energy constraints and in a limited fashion.

In Sec. II, we provide an update of the current status for weakly coupled, $q\bar{q}$, color-neutral vector resonances and discuss associated phenomenology that can further the experimental sensitivity in coming years. After introducing a minimal anomalon sector for gauged baryon number, in Sec. III we focus on the kinetic mixing operators between the new Z'_B boson and the Z and γ bosons of the SM induced by the anomalon content. The finite kinetic mixing effects from the UV completion of gauged baryon number are also important for the phenomenology of Z'_B bosons lighter than the Z boson. We reevaluate the constraints in the coupling-mass plane from mixing with the Z boson, Υ

meson, direct $q\bar{q}$ resonance limits from colliders, LEP limits on charged anomalon, and the anomaly-induced $Z \to Z'_B \gamma$ exotic decay in Sec. IV. We conclude in Sec. V, and a detailed discussion of our kinetic mixing calculation is presented in the Appendix.

II. DIJET RESONANCE LIMITS IN THE COUPLING-MASS PLANE

A color-singlet, electrically neutral spin-1 particle, usually referred to as a Z' boson, may have renormalizable couplings to the SM quarks. As we are interested in bosons of a wide range of masses, including at or below the electroweak scale, the simplest set of couplings is flavor diagonal and universal, as described by the following Lagrangian terms:

$$\frac{g_B}{2} Z'_{B\mu} \sum_q \left(\frac{1}{3} \bar{q}_L \gamma^\mu q_L + \frac{1}{3} \bar{q}_R \gamma^\mu q_R \right). \quad (2.1)$$

The overall coupling g_B is typically of the order of one or smaller. Its normalization (the factor of $1/2$) is chosen to be similar to the SM Z coupling (if the hypercharge coupling is ignored). The factor of $1/3$ is included to highlight that these couplings are proportional to the baryon number, which is $1/3$ for both left- and right-handed quarks. Furthermore, we consider a leptophobic Z', so its tree-level couplings to leptons are also proportional to the baryon number, which is 0 for leptons. We use the label Z'_B for the Z' boson that has the couplings proportional to the baryon number.

We emphasize, though, that baryon number does not play any significant role in this section. The flavor-independent couplings (2.1) are considered here because they are convenient for comparing the many existing hadron collider limits without having to analyze constraints from flavor-changing processes. Furthermore, the collider limits on Z'_B discussed later in this section depend mostly on the couplings to the u and d quarks, because the parton-distribution functions (PDFs) of the other quarks are much smaller. Adapting these collider limits on Z'_B to Z' bosons that have different couplings to the u and d quarks is also relatively straightforward, by a rescaling of the u/d PDF ratio.

The theory that includes Z'_B, which is a massive spin-1 particle, is well behaved at high energies only if Z'_B is a gauge boson or a bound state. Either way, additional fields must be present. Here, we will assume that any such fields that couple to Z'_B are sufficiently heavy (usually above $M_{Z'}/2$), so that the only tree-level two-body decays of the Z'_B boson are induced by Eq. (2.1).

To be more specific, we will focus on the case where Z'_B is the gauge boson associated with a $U(1)_B$ symmetry. Since Z'_B is massive, there must be a $U(1)_B$ symmetry-breaking sector. The simplest choice is a complex scalar ϕ

that is a SM gauge singlet and carries $U(1)_B$ charge. In addition, there must be some set of new fermions (anomalons) charged under $SU(2)_W \times U(1)_Y \times U(1)_B$ such that all gauge anomalies cancel [3,29,31,32]. Thus, the full Lagrangian of the renormalizable model discussed here comprises, besides the SM, the following sectors: the kinetic terms for Z' [which includes the interaction terms (2.1)], ϕ, and each anomalon, the potential for ϕ that spontaneously breaks $U(1)_B$, as well as Yukawa interactions of two anomalons with ϕ and of one anomalon and one SM fermion with the SM Higgs doublet.

We assume that the anomalon masses, which are mostly induced by ϕ, are heavier than $M_{Z'}/2$. The opposite case, where the anomalon masses are lighter than $M_{Z'}/2$, has a highly model-dependent phenomenology due to the cascade decays of Z'_B via pairs of anomalons [33]. Besides decays to anomalons, a Z' boson could, in principle, decay into additional particles beyond the SM, as studied, for example, in [34]; we will not consider that possibility in this work.

There are two types of Z'_B decay modes at tree level: into two jets and into $t\bar{t}$ if $M_{Z'} > 2m_t$. The branching fraction into two jets is given at leading order by

$$B(Z'_B \to jj) = \left[1 + \frac{1}{5} \left(1 + \frac{2m_t^2}{M_{Z'}^2} \right) \left(1 - \frac{4m_t^2}{M_{Z'}^2} \right)^{1/2} \right]^{-1}. \quad (2.2)$$

This branching fraction[1] approaches $5/6$ for $M_{Z'} \gg 2m_t$ and 1 for $M_{Z'} \lesssim 2m_t$. The ratio between the total width and mass of the Z'_B boson is $\Gamma_{Z'}/M_{Z'} \approx g_B^2/(24\pi)$ for $M_{Z'} \gg 2m_t$ and is $5/6$ of that for $M_{Z'} \lesssim 2m_t$.

The properties of Z'_B primarily depend on two parameters: the mass $M_{Z'}$ and the coupling g_B. It is natural, therefore, to present the collider limits in the $(M_{Z'}, g_B)$ plane [3]. The s-channel production cross section of Z'_B at hadron colliders is proportional to g_B^2 and quickly decreases with $M_{Z'}$. At leading order, Z'_B production proceeds from quark-antiquark initial states. At next-to-leading order (NLO) in QCD, there are also contributions from quark-gluon initial states. We have computed the Z'_B NLO production cross section at the LHC using the MadGraph_aMC@NLO code [35], with model files generated by FeynRules [36] (which uses the FeynArts package [37] for NLO corrections), and the PDF set NNPDF3.1 NLO [38] with $\alpha_s(M_Z) = 0.118$. The MadGraph_aMC@NLO default dynamical factorization and renormalization scale (which is determined by the p_T of the decay products) was used, so that α_s is evaluated at a scale that is event dependent.

The resulting cross sections are shown in Fig. 1 for a Z' gauge coupling fixed at $g_B = 0.3$. This value has been chosen for illustrative purposes; note that g_B is a free parameter of the order of one or smaller and that the Z'

---

[1]The $m_t/M_{Z'}$ dependence here corrects a typo from Eq. (7) in Ref. [3].
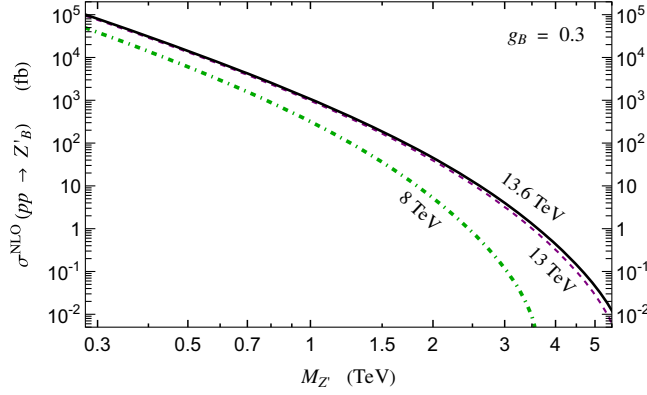
FIG. 1. Cross section for production of a Z'_B boson in proton-proton collisions at $\sqrt{s} = 13.6$ (solid black line), 13 (dashed purple line), and 8 TeV (green dash-dotted line). The coupling is fixed here at $g_B = 0.3$; the cross section scales as g_B^2. Next-to-leading-order QCD corrections are included through MadGraph_aMC@NLO.

production cross sections scale as g_B^2. The cross sections shown in Fig. 1 are computed for center of mass energies of 13.6 (the current one in run 3 of the LHC), 13 (used in run 2), and 8 TeV (used in run 1). The cross section is larger at $\sqrt{s} = 13.6$ TeV than at $\sqrt{s} = 13$ TeV by a factor that grows from 5% at $M_{Z'} = 0.1$ TeV to 9% at $M_{Z'} = 1$ TeV and 36% at $M_{Z'} = 4$ TeV.

The most stringent collider limits on the coupling for $M_{Z'} < 450$ GeV are set by LHC searches for a dijet resonance produced in association with an initial state jet, photon, or a leptonically decaying W boson. The production cross sections for $Z'_B j$ and $Z'_B \gamma$ at the 13.6 TeV LHC, computed at NLO with MadGraph_aMC@NLO, are shown in the left-hand panel in Fig. 2 for two choices of the p_T cut on the initial state radiation (ISR). The $Z'_B W$ production cross section times the W branching fraction into leptonic final states (excluding $\tau\nu$) is given in the right-hand panel in Fig. 2 by the dashed gray line.

We point out that additional processes that can be used in future searches at low dijet mass involve initial state radiation of a W or Z boson decaying hadronically. The cross section for Z'_B production in association with an electroweak boson that decays into jets is shown by the solid red line in the right-hand panel in Fig. 2. Note that at low mass this rate is larger by a factor of about 5 than the $Z'_B j$ rate with $p_{Tj} > 350$ GeV, so searches for associated $Z'_B W/Z$ production appear promising. The $Z'_B Z$ production cross section times the sum of Z branching fractions into e^+e^- and $\mu^+\mu^-$ is also given in the right-hand panel in Fig. 2 (see the dotted blue line). The low background for events with a leptonically decaying Z and a jj resonance would allow the use of $Z'_B Z$ production to improve the sensitivity to lower dijet masses.

Using an ISR jet as a trigger for light dijet resonances has been a key aspect for the current search sensitivity at low masses [7–9]. As a practical matter, however, the large boost to the Z'_B resonance necessitates the use of jet substructure techniques to both remove contamination from pileup and distinguish the Z'_B peak signal from the overwhelming QCD background. The p_T requirement from the ISR jet [7–9] thus leads to a sculpted invariant mass distribution, necessitating the use of novel experimental techniques to decorrelate the p_T of the ISR jet from the differential mass distribution [39].

The current coupling-mass limits are shown in Fig. 3 and are derived from various types of hadron collider searches, depending on the resonance mass. Only searches that set the most stringent limits for some mass range are included there [6,7,11,13–15,19,21,22]. Earlier limits that have been superseded can be found in [3].

For $M_{Z'} > 1.5$ TeV, the most stringent limits on g_B are set by dijet resonance searches at $\sqrt{s} = 13$ TeV. The CMS search [22] is based on the full run 2 luminosity, totaling 137 fb^{-1} of data (which supersedes the earlier high-mass results [19,20]). The ATLAS search [21] is also based on the full run 2 luminosity, totaling 139 fb^{-1} of data.
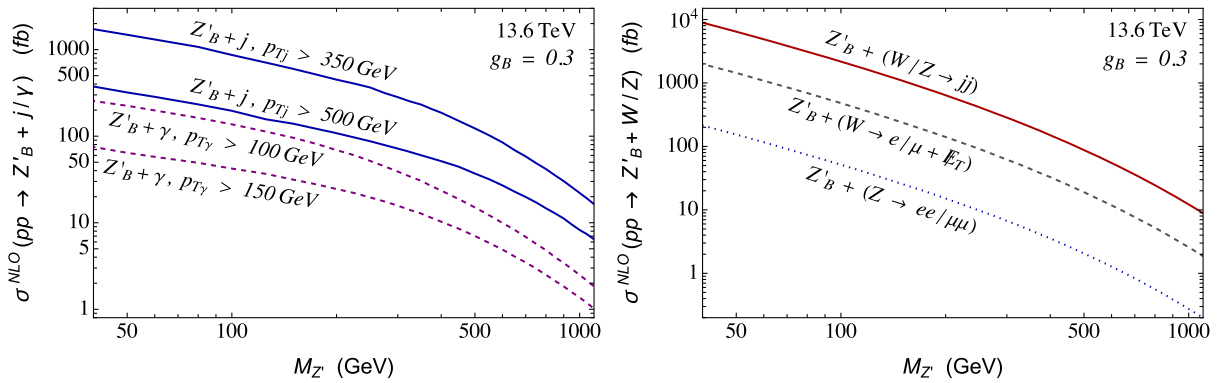

FIG. 2. Next-to-leading-order cross section for a Z'_B boson produced at the 13.6 TeV LHC in association with a jet (solid blue lines) or photon (dashed purple lines) of transverse momentum above a certain limit (left panel) or with a weak boson decaying to jets or leptons (right panel). The coupling used here is $g_B = 0.3$; all cross sections scale as g_B^2.
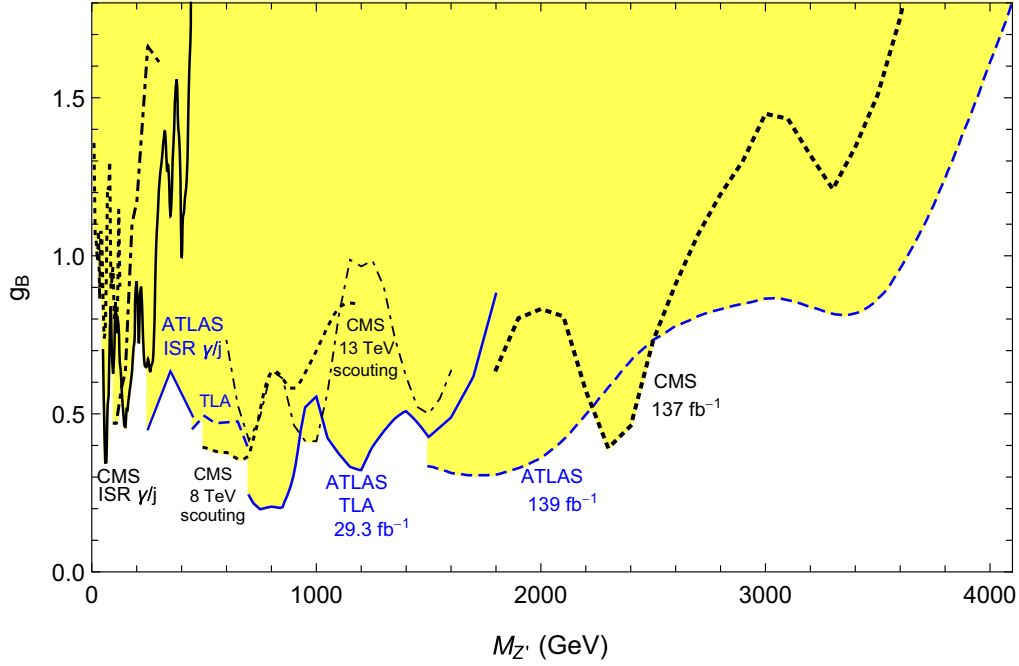
FIG. 3. Limits on the Z'_B boson in the coupling-mass plane, based on the ATLAS and CMS searches [6,7,11,13–15,19,21,22] described in the text. The yellow shaded region is excluded at the 95% confidence level. The normalization of the g_B coupling used here is given in Eq. (2.1).

These limits assume that the dijet signal is given by the Z'_B production cross section times the branching fraction $B(Z'_B \to jj)$ given in Eq. (2.2). In practice, for $M_{Z'} \gg 2m_t$ there is an additional contribution from $Z'_B \to t\bar{t}$, because each top quark is highly boosted and may appear as a jet. This effect is weaker in the case of ATLAS searches, where the jet cone size is $R = 0.5$, significantly smaller than the one used in CMS dijet searches, $R = 1.1$. The $t\bar{t}$ invariant mass distribution matches the dijet one only when both top quarks decay hadronically; otherwise, the neutrinos shift the invariant mass below $M_{Z'}$. Thus, the effective dijet branching fraction of Z'_B is slightly higher than $5/6$, reaching $5/6 + B(W \to jj)^2/6 \approx 0.91$ at very high masses. Consequently, the limits on g_B may be up to 5% tighter than those shown in Fig. 3.

For $450 \text{ GeV} < M_{Z'} < 1.5 \text{ TeV}$, there is competition between four searches. The CMS method in that mass range, called "scouting," uses dijets reconstructed from calorimeter information in the trigger. The latest CMS search of this type uses 27 fb^{-1} of 13 TeV data (the low-mass result of [19]) and sets a competitive limit especially in the 0.9–1 TeV mass range, while the search with 18.8 fb^{-1} of 8 TeV data [6] still sets the most stringent limit in the 500–700 GeV mass range. The similar ATLAS "trigger-level analysis" (TLA) used 29.3 fb^{-1} of 13 TeV data [11], setting the most stringent limit in the 700–900 GeV and 1–1.5 TeV mass ranges; a version of that search [11] with a different event selection and only 3.4 fb^{-1} sets the most stringent limit in the 450–500 GeV mass range.

In the 237–450 GeV mass range, the best limits are set by the ATLAS searches with ISR of a jet or a photon (79.8 fb^{-1} at 13 TeV [13]) and b-tagged jets. The ATLAS 139 fb^{-1} search using an ISR W boson giving a high-p_T lepton for the trigger [40] gives a slightly weaker bound.

Finally, for 50–237 GeV, the limit is set for most Z'_B masses by the CMS search for a dijet resonance plus an ISR jet with 35.9 fb^{-1} accumulated in 2016 [15], where the dijet system is boosted and merged into a single jet with substructure. In the relatively narrow 100–135 GeV mass range, the strongest limit is set by the similar CMS search with the 2015 data of 2.7 fb^{-1} [7]. From 10–50 GeV, the CMS analysis with an ISR photon with 35.9 fb^{-1} [14] gives the leading direct constraint on dijet resonances.

The coupling-mass plot in Fig. 3 shows that there is a gap in sensitivity for $M_{Z'}$ roughly in the 200–500 GeV range. Improved techniques will be required to fill that gap. By contrast, the high-mass region will continue to be covered by existing analyses applied to larger datasets. Higher-energy proton-proton colliders will substantially increase the reach at high $M_{Z'}$ [41].

At the other end of the plot, masses below 100 GeV are also constrained by electroweak precision and quarkonium measurements. We will next derive these constraints by calculating the mixing of the Z' with SM states.

III. Z'_B MIXING WITH THE Z AND THE PHOTON

Besides the limits from hadron collider searches discussed in the previous section, there are constraints on the

Z'_B boson from measurements of the Z boson properties. The mixing between the SM Z boson (labeled here Z_{SM}) and the Z'_B boson may modify the branching fractions of the observed Z boson compared to the SM predictions at a level incompatible with existing measurements. Furthermore, the $Z'_B - Z_{\mathrm{SM}}$ mixing as well as the kinetic mixing between the Z'_B and the photon lead to Z'_B decays into pairs of leptons [33], which are constrained by searches for dilepton resonances.

A kinetic mixing between the SM hypercharge gauge boson and the Z'_B may, in principle, be present at tree level. If, however, the $U(1)_Y$ or the $U(1)_B$ gauge groups are embedded in a non-Abelian structure at some high scale (which is generically expected as they are not asymptotically free), then the tree-level kinetic mixing vanishes.

Nevertheless, a $Z'_B - Z_{\mathrm{SM}}$ mixing will be generated by loops involving fields that couple to both bosons. To compute the one-loop $Z'_B - Z_{\mathrm{SM}}$ mixing, we first need to specify all the fields that carry electroweak charges and also couple to Z'_B.

A. Kinetic mixing

Let us consider in what follows the theory where Z'_B is the gauge boson associated with a $U(1)_B$ gauge symmetry, so that Z'_B does not couple to leptons while its couplings given in Eq. (2.1) arise when all SM quarks carry the same $U(1)_B$ charge, chosen to be $1/3$. The gauge theory with these quark charges is not self-consistent unless certain new fermions, called anomalons, are present to cancel the gauge anomalies. If some of these have masses below $M_{Z'}/2$, then the Z'_B can decay into anomalon pairs, leading to interesting collider signatures [32].

We focus on sets of anomalons which together with the SM quarks satisfy the orthogonality condition $\mathrm{Tr}(YB) = 0$, where the trace is over all fields, Y is the hypercharge, and B is the $U(1)_B$ charge. More explicitly, the condition is

$$\sum_{f=\mathrm{quarks,anom}} N_f(Y_L^f B_L^f + Y_R^f B_R^f) = 0, \quad (3.1)$$

where the sum is over the fermions f, which are all the anomalons and the SM quarks in the gauge eigenstate basis, Y_L^f and B_L^f are the hypercharge and $U(1)_B$ charge, respectively, of the left-handed f fermion, and Y_R^f and B_R^f are the corresponding charges of the right-handed fermions. The color factor is $N_f = 3$ when f is a quark and $N_f = 1$ when f is a color-singlet fermion. When the above equation is satisfied, the leading one-loop contribution to the kinetic mixing between the SM hypercharge gauge boson and the Z'_B vanishes, so the constraint from Z measurements is weak.

Kinetic mixing operators are still generated at one loop due to the mass differences between anomalons and SM

quarks. The leading operators of this type [33] have dimension six and involve the SM Higgs doublet H or the $U(1)_B$-breaking scalar ϕ:

$$\phi^\dagger \phi Z'_{B\mu\nu} B^{\mu\nu}, \qquad H^\dagger H Z'_{B\mu\nu} B^{\mu\nu}, \qquad H^\dagger \tau^a H Z'_{B\mu\nu} W^{a\mu\nu}, \quad (3.2)$$

where $B^{\mu\nu}$ and $W^{a\mu\nu}$ are the hypercharge and $SU(2)_W$ field strengths, respectively.

There are also mass mixing operators, which arise at dimension six:

$$H^\dagger(D^\mu H)\phi(D_\mu \phi^\dagger) + \mathrm{H.c.}, \qquad H^\dagger(D^\mu H)\phi^\dagger(D_\mu \phi) + \mathrm{H.c.} \quad (3.3)$$

These may arise at one loop, depending on the anomalon charges. Once a Higgs doublet and a ϕ scalar are replaced by their vacuum expectation values (VEVs), a $Z'_B - Z_{\mathrm{SM}}$ mass mixing is induced.

As the masses of the Z'_B and the anomalons may be at or below the weak scale, it is appropriate to compute the mixings of Z'_B with the Z_{SM} and the photon rather than the ones involving the $SU(2)_W \times U(1)_Y$ gauge bosons. The Lagrangian terms for these can be written as

$$\frac{1}{2} Z'^{\mu\nu}_B (\kappa_Z Z_{\mathrm{SM}\mu\nu} - \kappa_\gamma F_{\mu\nu}) + \Delta M^2_{Z'Z} Z'^\mu_B Z_{\mathrm{SM}\mu}, \quad (3.4)$$

where the coefficients κ_Z and κ_γ are dimensionless and real and $\Delta M^2_{Z'Z}$ is a mass-squared parameter. The field strengths for Z'_B, Z_{SM}, and the photon are canonically normalized; i.e., the tree-level kinetic terms are $(-1/4)(Z'^{\mu\nu}_B Z'_{B\mu\nu} + Z^{\mu\nu}_{\mathrm{SM}} Z_{\mathrm{SM}\mu\nu} + F^{\mu\nu} F_{\mu\nu})$.

The real part of the $Z'_B - Z_{\mathrm{SM}}$ mixing amplitude contains two pieces: a kinetic mixing and a mass mixing. The $Z'_B - Z_{\mathrm{SM}}$ mixing amplitude can be written as $\epsilon_\mu(Z'_B)\epsilon_\nu(Z)\mathcal{A}^{\mu\nu}_{Z'Z}$, with $\epsilon_\mu(Z'_B)$ and $\epsilon_\nu(Z)$ being the polarization vectors of the two gauge bosons. The real part of $\mathcal{A}^{\mu\nu}_{Z'Z}$ is

$$\mathrm{Re}\mathcal{A}^{\mu\nu}_{Z'Z} = \kappa_Z(g^{\mu\nu}p^2 - p^\mu p^\nu) + \Delta M^2_{Z'Z} g^{\mu\nu}, \quad (3.5)$$

where p^μ is the 4-momentum of the Z'_B or Z_{SM} bosons.

The sine and cosine of the weak mixing angle are labeled in what follows by s_W and c_W, while the $SU(2)_W$ gauge coupling is $g = e/s_W$, where e is the electromagnetic gauge coupling. Expressing the Z_{SM} couplings of the left- and right-handed fermion f (without the g/c_W prefactor) in terms of their T^3 value and hypercharge,

$$g_{L,R}^f = c_W^2 T_{L,R}^3 - s_W^2 Y_{L,R}^f, \quad (3.6)$$

we find that the sum of the Z_{SM} couplings over the fermions belonging to an $SU(2)_W$ multiplet of size n is proportional to the hypercharge Y^f of that representation:

$$\sum_{f \in n} g_{L,R}^f = -n s_W^2 Y_{L,R}^f. \tag{3.7}$$

From Eq. (3.1) then follows an important sum rule:

$$\sum_{f=\text{quarks, anom}} N_f (g_L^f B_L^f + g_R^f B_R^f) = 0. \tag{3.8}$$

If all the SM quarks and anomalons had the same mass, then Eq. (3.8) would have implied that the $Z_B' - Z_{SM}$ kinetic mixing vanishes at one loop. As the top quark is much heavier than the other SM quarks, the kinetic mixing receives a significant contribution from the SM. The anomalons also contribute to the kinetic mixing, with an amount sensitive to the anomalon masses and also to the anomalon charges. The dependence of the kinetic mixing on the anomalon set has not been recognized in previous work [24,26,27,31,42]. Similarly, the fact that the loop-induced kinetic mixing is finite has been mostly overlooked (an exception is [33]).

To be concrete, we analyze a renormalizable Lagrangian that includes the SM plus the canonical kinetic terms for the $U(1)_B$ gauge boson, for a complex scalar ϕ of $U(1)_B$ charge $+3$, and for a minimal set of anomalons that satisfies the trace condition (3.8), as well as a ϕ potential and Yukawa couplings. There are no tree-level kinetic or mass mixings involving the fields beyond the SM. Fermion loops will generate kinetic mixing but no independent $\Delta M_{Z'Z}^2$ mass mixing, because the anomalons are vectorlike with respect to the SM gauge group.

In the Appendix, we compute the mixing between Z_{SM} and any Z' induced at one loop by any fermions that satisfy an orthogonality relation like (3.8). In this section, we are primarily interested in the case where the 4-momentum of the gauge bosons satisfies $p^2 = M_Z^2$, so that we can extract limits on the Z' from measurements at the Z pole. The one-loop computations of the mixings are simplified when the anomalon couplings to the Higgs doublet are negligible; i.e., the anomalon masses come entirely from Yukawa couplings to the scalar ϕ responsible for spontaneously breaking $U(1)_B$. In that situation, there are no one-loop contributions to $\Delta M_{Z'Z}^2$, because the operators (3.3) cannot be generated either by SM quarks (which do not couple to ϕ) or by anomalons (which do not couple to H). This can also be seen from (A6), which gives $\Delta M_{Z'Z}^2$ after setting $z_L^q = z_R^q$ for the SM quarks and $g_L^f = g_R^f$ for the anomalons.

The expansion in (A10) shows that the loops involving the SM quarks other than the top quark have contributions to the kinetic mixing which are of the order of $(m_q/M_Z)^2$, where m_q are the SM quark masses, and, thus, can be neglected. Hence, the kinetic mixing, given, in general, in (A9), becomes a sum over the top quark and anomalon contributions:

$$\kappa_Z \simeq \frac{g_B g}{48\pi^2 c_W} \left[\left(\frac{1}{2} - \frac{4}{3} s_W^2 \right) \mathcal{F}(m_t^2/M_Z^2) \right.$$
$$\left. + \sum_{f=\text{anom}} N_f (g_L^f B_L^f + g_R^f B_R^f) \mathcal{F}(m_f^2/M_Z^2) \right]. \tag{3.9}$$

The function $\mathcal{F}$ is given in Eq. (A8) in the Appendix and for $m_f \gtrsim M_Z$ is well approximated by

$$\mathcal{F}(m_f^2/M_Z^2) \simeq 2 \ln\left(\frac{m_f}{M_Z} \right) + \frac{5}{3} - \frac{M_Z^2}{5 m_f^2}. \tag{3.10}$$

For m_f in the interval 100–400 GeV, $\mathcal{F}(m_f^2/M_Z^2)$ continuously grows from 1.67 to 4.61.

As mentioned in Sec. II, we will focus here on the case where all the anomalons are color singlets ($N_f = 1$) and heavier than $M_{Z'}/2$, where $M_{Z'}$ is the mass of the physical particle Z'. The collider constraints on the anomalons are weak in this case: Pair production at LEP II sets a lower limit on the anomalon mass of about 90 GeV, depending on the anomalon decay modes [31]. Using (3.7) and replacing the known quantities in Eq. (3.9) by their numerical values, we find the following expression for the $Z_B' - Z_{SM}$ kinetic mixing at one loop:

$$\kappa_Z \simeq 8.70 \times 10^{-4} g_B \left(1 - 0.417 \sum_{f=\text{anom}} Y^f \right.$$
$$\left. \times (B_L^f + B_R^f) \mathcal{F}(m_f^2/M_Z^2) \right). \tag{3.11}$$

The same computation detailed in the Appendix, but with the Z couplings replaced by the photon ones, gives the following expression for the kinetic mixing of the Z_B' with the SM photon, defined in (3.4):

$$\kappa_\gamma \simeq \frac{-g_B e}{48\pi^2} \left[\frac{4}{3} \mathcal{F}(m_t^2/M_{Z'}^2) \right.$$
$$\left. + \sum_{f=\text{anom}} Q^f (B_L^f + B_R^f) \mathcal{F}(m_f^2/M_{Z'}^2) \right]. \tag{3.12}$$

A minimal set of anomalons which includes only color singlets, cancels all gauge anomalies, and satisfies the trace condition is given by the following $SU(2)_W \times U(1)_Y \times U(1)_B$ representations [29,31,32]:

$$L_L(2, -1/2, -1), \qquad L_R(2, -1/2, 2),$$
$$E_L(1, -1, 2), \qquad E_R(1, -1, -1)$$
$$N_L(1, 0, 2), \qquad N_R(1, 0, -1). \tag{3.13}$$

The SM gauge singlet fermions N_L and N_R are required to cancel the $U(1)_B$ and $[U(1)_B]^3$ anomalies but do not contribute to the kinetic mixing. The anomalons acquire mass from the scalar ϕ, with $U(1)_B$ charge $+3$ and whose VEV $\langle\phi\rangle = v_\phi$ breaks the $U(1)_B$ symmetry. The corresponding Yukawa interactions

$$-y_L \bar{L}_L \phi^* L_R - y_E \bar{E}_L \phi E_R - y_N \bar{N}_L \phi N_R + \text{H.c.} \quad (3.14)$$

set the anomalon masses to be $y_L v_\phi$, $y_E v_\phi$, and $y_N v_\phi$. We assume the dominant mass generation arises from $U(1)_B$ breaking and neglect the possible Yukawa interactions to the SM Higgs doublet. We remark that small Yukawa interactions to the SM Higgs doublet, which are needed to ensure the charged anomalons can decay to SM fermions, are still allowed by $h \to \gamma\gamma$ constraints [43]. These and other Higgs observables also exclude some of the original models for local baryon number [24,25]. If all anomalons have the same mass, $m_f \gtrsim 90$ GeV, then the anomalon-dependent factor in (3.11) becomes

$$\sum_{f=\text{anom}} Y^f (B^f_L + B^f_R) \mathcal{F}(m^2_f/M^2_Z) = -2\mathcal{F}(m^2_f/M^2_Z), \quad (3.15)$$

and we obtain that this anomalon set gives $\kappa_Z/g_B \simeq 2.08 \times 10^{-3}$ for $m_f = 100$ GeV and $\kappa_Z/g_B \simeq 3.19 \times 10^{-3}$ for $m_f = 200$ GeV. Under the same assumptions, the photon kinetic mixing in (3.12) with $M_{Z'} \approx M_Z$ gives $\kappa_\gamma/g_B \simeq -3.32 \times 10^{-4}$ for $m_f = 100$ GeV and $\kappa_\gamma/g_B \simeq 1.69 \times 10^{-3}$ for $m_f = 200$ GeV. The values for κ_γ and κ_Z are roughly comparable, because both originate from a single kinetic mixing of the hypercharge gauge field with the Z'_B field.

B. Couplings of the physical bosons

We now diagonalize the kinetic terms for the Z_{SM}, Z'_B bosons, and the photon, including the mixing terms from (3.4). Given that the kinetic mixing with the photon has only a subdominant impact on phenomenology (due to the tree-level couplings of Z'_B to quarks), it is convenient to work in the leading order in $\kappa_\gamma \ll 1$. It is then sufficient to redefine Z_{SM} and Z'_B first to absorb the kinetic mixing κ_Z, where the nonunitary nature of the field redefinition induces mass mixing between the two heavy bosons. The induced mass mixing is symmetric and requires one rotation angle to obtain diagonal mass eigenstates. The kinetic mixing with the photon is absorbed by a redefinition of the photon field by $\kappa_\gamma Z'_B$, which leads to Z'_B couplings to the electromagnetic current proportional to κ_γ and no further mass mixing, as studied in Ref. [33]. A more general diagonalization of the kinetic mixing between Z_{SM}, Z'_B, and the photon can be found in Ref. [44].

Combining the field redefinition of Z_{SM} and Z'_B and mass diagonalization attributed to κ_Z, we find that the mass eigenstate bosons, labeled by Z and Z', are

$$Z^\mu = \cos\theta Z^\mu_{\text{SM}} + \left(\sin\theta\sqrt{1-\kappa^2_Z} - \kappa_Z\cos\theta\right)Z'^\mu_B,$$

$$Z'^\mu = \left(\cos\theta\sqrt{1-\kappa^2_Z} + \kappa_Z\sin\theta\right)Z'^\mu_B - \sin\theta Z^\mu_{\text{SM}}, \quad (3.16)$$

where $-\pi/4 < \theta < \pi/4$ and

$$\tan 2\theta = \frac{2\kappa_Z}{1 - 2\kappa^2_Z - M^2_{Z'_B}/M^2_{Z_{\text{SM}}}}\sqrt{1-\kappa^2_Z}. \quad (3.17)$$

The squared masses of the two physical states are

$$M^2_{Z,Z'} = \frac{1}{2(1-\kappa^2_Z)}\left(M^2_{Z_{\text{SM}}} + M^2_{Z'_B}\right.$$
$$\left. \pm \sqrt{(M^2_{Z_{\text{SM}}} - M^2_{Z'_B})^2 + 4\kappa^2_Z M^2_{Z_{\text{SM}}} M^2_{Z'_B}}\right), \quad (3.18)$$

where the $+$ sign corresponds to M^2_Z only when $M_{Z_{\text{SM}}} \geq M_{Z'_B}$. Since $\kappa_Z \ll 1$, in what follows we drop the terms of the order of κ^2_Z from Eq. (3.16) and from the prefactor in Eq. (3.18). As the Z'_B mass may be close to $M_{Z_{\text{SM}}}$, we do not yet expand the denominator in Eq. (3.17) or the last term in Eq. (3.18).

As a consequence of mixing, the couplings of the physical Z boson to quarks and leptons are changed compared to the SM ones, given in Eq. (3.6), as follows:

$$g^q_{L,R} \to \hat{g}^q_{L,R} = (\cos\theta + \kappa_Z\sin\theta)g^q_{L,R} + \sin\theta\frac{g_B c_W}{6g},$$

$$g^\ell_{L,R} \to \hat{g}^\ell_{L,R} = (\cos\theta + \kappa_Z\sin\theta) g^\ell_{L,R}. \quad (3.19)$$

The couplings of the physical Z' boson to quarks are modified compared to those of Z'_B gauge boson shown in Eq. (2.1), by a charge- and chirality-dependent factor:

$$\cos\theta + (-\sin\theta + \kappa_Z\cos\theta)\frac{6g}{g_B c_W} g^q_{L,R}. \quad (3.20)$$

In addition, the $Z'_B - Z_{\text{SM}}$ kinetic mixing induces couplings of Z' to leptons:

$$Z'_\mu\frac{g}{c_W}(-\sin\theta + \kappa_Z\cos\theta)\sum_\ell(g^\ell_L\bar{\ell}_L\gamma^\mu\ell_L + g^\ell_R\bar{\ell}_R\gamma^\mu\ell_R).$$
$$(3.21)$$

The kinetic mixing between Z'_B and the photon, κ_γ, which is given in (3.12), also contributes to the Z' couplings to leptons, as studied in Ref. [33]. Note, however, that the couplings of Z' to leptons are both loop suppressed and proportional to g_B, so that the branching fractions of the Z' into leptons are at the subpercent level and would become relevant only after the Z' discovery via the quark-antiquark modes.

C. Limits from electroweak measurements

Let us focus first on the typical case, where the relative mass splitting of the two gauge bosons is large compared to the kinetic mixing: $|M_{Z'_B} - M_{Z_{SM}}| \gg \kappa_Z M_{Z_{SM}}$. In that case, Eq. (3.17) implies $\sin\theta \ll 1$ and, to leading order in κ_Z^2,

$$\sin\theta \simeq \frac{\kappa_Z}{1 - M_{Z'}^2/M_Z^2}. \quad (3.22)$$

Furthermore, the mass difference between the two physical particles in this case is approximately equal to the mass difference of the two gauge bosons: $M_{Z'} - M_Z \simeq M_{Z'_B} - M_{Z_{SM}}$ up to corrections of the order of $(\kappa_Z M_{Z_{SM}})^2/(M_{Z'_B} - M_{Z_{SM}})^2$. The constraints from Z pole measurements depend on the size of the $M_{Z'} - M_Z$ mass splitting compared to the measured Z width, $\Gamma_Z \approx 2.5$ GeV.

When $|M_{Z'} - M_Z| \gtrsim \Gamma_Z$, the contribution from Z' exchange to the Z pole observables can be neglected. In that case, the main effect of the $Z'_B - Z_{SM}$ kinetic mixing is a relative change in the hadronic Z width compared to the SM prediction:

$$\frac{\Delta\Gamma_{\text{had}}(Z)}{\Gamma_{\text{had}}^{\text{SM}}(Z)} = \frac{3[(\hat{g}_L^d)^2 + (\hat{g}_R^d)^2] + 2[(\hat{g}_L^u)^2 + (\hat{g}_R^u)^2]}{3[(g_L^d)^2 + (g_R^d)^2] + 2[(g_L^u)^2 + (g_R^u)^2]} - 1$$

$$\simeq -\frac{A_1 g_B \kappa_Z}{1 - M_{Z'}^2/M_Z^2}, \quad (3.23)$$

where the coefficient A_1 is a function of the weak mixing angle:

$$A_1 = \left(\frac{c_W}{6g}\right)\frac{1 + 4s_W^2/3}{5/4 - 7s_W^2/3 + 22s_W^4/9} \approx 0.349. \quad (3.24)$$

Note that the correction to the leptonic Z width is of the order of $\sin^2\theta$ and can be neglected here. For the anomalon set (3.13), with a common mass fixed at $m_f = 100$ GeV, the constraint becomes

$$\frac{\Delta\Gamma_{\text{had}}(Z)}{\Gamma_{\text{had}}^{\text{SM}}(Z)} \simeq -7.25 \times 10^{-4} \frac{g_B^2}{1 - M_{Z'}^2/M_Z^2}. \quad (3.25)$$

The value for the hadronic Z width obtained from a fit [45] to the LEP I and SLC data is $\Gamma_{\text{had}}(Z) = 1.7444 \pm 0.0020$ GeV, while the SM prediction is $\Gamma_{\text{had}}^{\text{SM}}(Z) = 1.7411 \pm 0.0008$ GeV. The allowed interval for the relative change in the hadronic Z width, at the 95% CL, is

$$-5.30 \times 10^{-4} < \frac{\Delta\Gamma_{\text{had}}(Z)}{\Gamma_{\text{had}}^{\text{SM}}(Z)} < 4.30 \times 10^{-3}. \quad (3.26)$$

Comparing this interval with Eq. (3.25) leads to the following upper limit on the $U(1)_B$ gauge coupling:

$$g_B < \begin{cases} 0.855\left(1 - \frac{M_{Z'}^2}{M_Z^2}\right)^{1/2}, & \text{for } M_{Z'} \lesssim M_Z - \Gamma_Z, \\ 2.44\left(\frac{M_{Z'}^2}{M_Z^2} - 1\right)^{1/2}, & \text{for } M_{Z'} \gtrsim M_Z + \Gamma_Z, \end{cases} \quad (3.27)$$

assuming the anomalon set (3.13) with a common anomalon mass $m_f = 100$ GeV. For $m_f = 200$ GeV, the limit on g_B is multiplied by 0.808. For other anomalon charges or masses, the right-hand side of (3.27) is multiplied by $(2.08 \times 10^{-3} g_B/\kappa_Z)^{1/2}$, where κ_Z is given in Eq. (3.11).

When the Z' mass is approximately within one Z width from the Z mass, i.e., in the interval 88.7 GeV $\lesssim M_{Z'} \lesssim 93.7$ GeV, Z' exchange also contributes to processes such as $e^+e^- \to$ hadrons near the Z pole. In that case, the interference between the Z and Z' exchange amplitudes leads to corrections of the cross section for $e^+e^- \to$ hadrons near the Z pole, σ_{had}, which are not limited to just $\Gamma_{\text{had}}(Z)$. The relative change of σ_{had} compared to the SM prediction is approximately given by

$$\frac{\Delta\sigma_{\text{had}}}{\sigma_{\text{had}}^{\text{SM}}} \simeq -\frac{A_1 g_B \kappa_Z}{1 - M_{Z'}^2/M_Z^2}\left(1 - \frac{\Gamma_Z \Gamma_{Z'}}{4(M_Z - M_{Z'})^2 + \Gamma_{Z'}^2}\right). \quad (3.28)$$

To derive this, we took the energy of the e^+e^- collision to be $\sqrt{s} = M_Z$. The last term in the parentheses is due to interference and depends on the total width of the Z' boson: $\Gamma_{Z'} \simeq (5/6)g_B^2 M_{Z'}/(24\pi)$ to leading order in $\sin\theta$. The fit to the LEP I and SLD data gives $\sigma_{\text{had}} = 41.541 \pm 0.037$ nb, which is 1.6σ higher than the SM prediction, $\sigma_{\text{had}}^{\text{SM}} = 41.481 \pm 0.008$ nb [45]. As a consequence, the lower limit on σ_{had} is particularly tight at the 95% CL:

$$-3.42 \times 10^{-4} < \frac{\Delta\sigma_{\text{had}}}{\sigma_{\text{had}}^{\text{SM}}} < 3.24 \times 10^{-3}. \quad (3.29)$$

Comparing this interval with Eq. (3.28) gives a nonlinear constraint on g_B as a function of $M_{Z'}$, which applies to the $M_Z - \Gamma_Z \lesssim M_{Z'} \lesssim M_Z + \Gamma_Z$ range except for a very narrow region centered around M_Z:

$$g_B^2 - \left[\left(\frac{1 - M_{Z'}/M_Z}{8.70 \times 10^{-3} g_B^2}\right)^2 + 0.404\right]^{-1}$$

$$< \begin{cases} 0.944\left(1 - \frac{M_{Z'}}{M_Z}\right), & \text{for } \kappa_Z \lesssim 1 - \frac{M_{Z'}}{M_Z} \lesssim \frac{\Gamma_Z}{M_Z}, \\ 8.93\left(\frac{M_{Z'}}{M_Z} - 1\right), & \text{for } \kappa_Z \lesssim \frac{M_{Z'}}{M_Z} - 1 \lesssim \frac{\Gamma_Z}{M_Z}. \end{cases} \quad (3.30)$$

Here, we used the anomalon set (3.13) with a common mass fixed at $m_f = 100$ GeV. We will use the above constraint as well as Eq. (3.27) when we extend the coupling-mass plot at low masses in Sec. IV. For $m_f = 200$ GeV, the right-hand side of (3.30) must be multiplied by a factor

of 0.652, while for other anomalon masses or charges the factor is $2.08 \times 10^{-3} g_B/\kappa_Z$.

For $|M_{Z'} - M_Z| \lesssim \kappa_Z M_Z$, the one-loop mixing between Z'_B and $Z_{\rm SM}$ in Eq. (3.17) is large, $\sin\theta \approx 1/\sqrt{2}$, as also discussed in Ref. [44]. Because the diagonalization to the mass basis considers only the pole terms in the one-loop wave function correction, the evaluation of the one-loop diagrams cannot be neglected in scattering cross sections. The mass shift of the $Z_{\rm SM}$ boson from a Z' close in mass was used before as the constraint on κ_Z [46], but that result needs to be revisited for the very narrow region where the relative mass difference is below κ_Z. In particular, the one-loop interference in scattering processes with $|M_{Z'} - M_Z| \lesssim \kappa_Z M_Z$ leads to interesting new phenomenology akin to neutral meson mixing, which we reserve for future study.

IV. LOW-MASS CONSTRAINTS IN THE MINIMAL Z'_B MODEL

The coupling-mass plot is very useful for displaying the LHC dijet resonance limits. Its linear-linear version (see Fig. 3), however, does not clearly show the limits for new bosons at or below the electroweak scale.

By contrast, the log-log version of the coupling-mass plot, shown in Fig. 4, clearly displays the low-mass region. The yellow-shaded region is excluded at the 95% confidence level by dijet resonance searches at the LHC (and is identical to the shaded region from Fig. 3). The gray-shaded region labeled "Z width" is ruled out by measurements of the hadronic Z width, which would be modified by the Z–Z'_B mixing induced at one loop by the SM quarks and also by the anomalons. The boundary of that region is the limit on the Z'_B coupling, g_B, given in (3.27) for a common anomalon mass of 100 GeV. For other anomalon masses, the limit changes as described after (3.27), and the bound for a common anomalon mass of 200 GeV is shown as a dotted line for concreteness. The limit is more complicated [see (3.30) and the text after that] when $|M_{Z'} - M_Z| \lesssim \Gamma_Z$, due to interference effects in the cross section for $e^+ e^- \to$ hadrons.

The gray-shaded region labeled "$\Upsilon \to jj$" in Fig. 4 is excluded by the search for nonelectromagnetic decays of Υ into a jet pair performed by the ARGUS Collaboration [47]. This constraint is related to the ratio $R_\Upsilon = \Gamma(\Upsilon \to {\rm hadrons})/\Gamma(\Upsilon \to \mu^+\mu^-)$. To evaluate R_Υ in the SM, we must include the three-gluon final state in the hadronic width as well as photon and Z-mediated dijet and dimuon production [48,49]. Since the Z-mediated interference and contribution to the dimuon width is an $\mathcal{O}(10^{-3})$ correction to the QED contribution, we treat the dimuon width as a purely QED calculation for both the SM and baryon-number calculation of R_Υ. Consequently, the $|\Delta R_\Upsilon| = |R_\Upsilon - R_\Upsilon^{\rm SM}|$ absolute difference cancels the
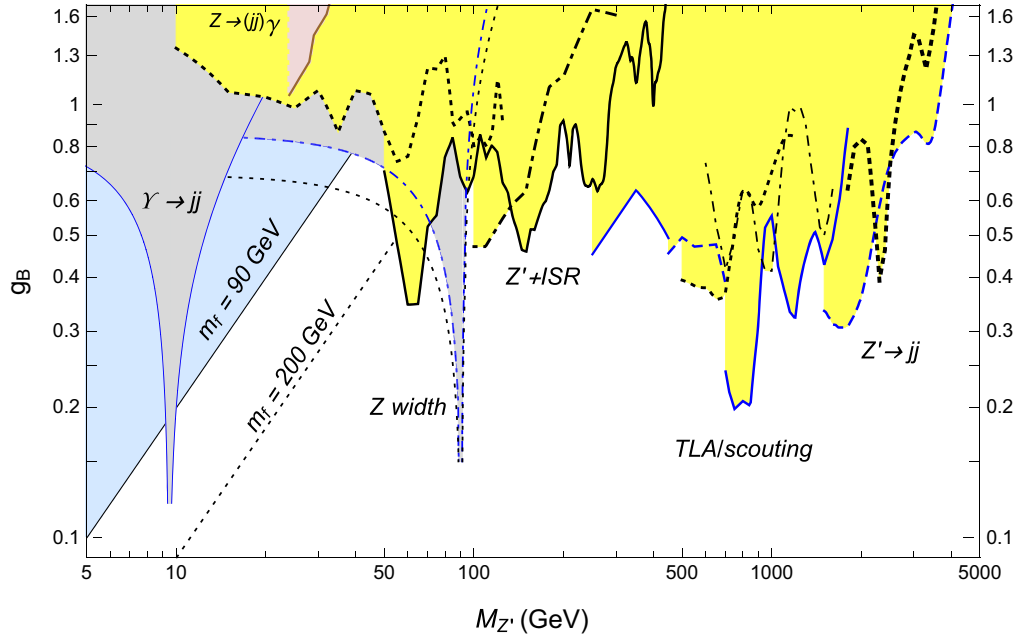

FIG. 4. Limits on the Z'_B boson in the log-log coupling-mass plane. The yellow-shaded region is excluded at the 95% confidence level by dijet resonance searches at the LHC (see Fig. 3). The gray-shaded regions (which are particularly strong near 91.2 and 9.5 GeV) are excluded by measurements of the Z hadronic width at LEP I (the upper dot-dashed line corresponds to an anomalon mass $m_f = 100$ GeV and the lower dotted line to $m_f = 200$ GeV) and by the ARGUS search for nonelectromagnetic Υ decay into a jet pair. The blue-shaded region (above the solid straight line) is ruled out by the lower limit on anomalon masses in conjunction with the theoretical upper limit on Yukawa couplings, and the dotted straight line indicates the possible exclusion if the anomalon mass constraint is increased to 200 GeV. The pink-shaded region labeled $Z \to (jj)\gamma$ is excluded by the L3 search for $Z \to Z'\gamma \to (jj)\gamma$.

three-gluon contribution to the hadronic width, so the modification of the dijet width provides the leading sensitivity to the parameters g_B and $M_{Z'}$. The ARGUS constraint on the nonelectromagnetic dijet decays of Υ gives $|\Delta R_\Upsilon| < 2.1$.

Thus, we calculate

$$\Delta R_\Upsilon = \frac{\sum_q (|\mathcal{M}_\gamma(q\bar{q}) + \mathcal{M}_Z(q\bar{q}) + \mathcal{M}_{Z'}(q\bar{q})|^2 - |\mathcal{M}_\gamma(q\bar{q}) + \mathcal{M}_{Z_{SM}}(q\bar{q})|^2)}{|\mathcal{M}_\gamma(\mu^+\mu^-)|^2}, \qquad (4.1)$$

where $\mathcal{M}_Z(q\bar{q})$ uses the modified Z couplings, Eq. (3.19). In the limit that the Υ decay products are massless and $Z'_B - Z_{SM}$ kinetic mixing is neglected, we obtain

$$\Delta R_\Upsilon = \frac{g_B^2 M_\Upsilon^2}{3e^2(M_{Z'}^2 - M_\Upsilon^2)}\left(1 + \frac{g_B^2 M_\Upsilon^2}{4e^2(M_{Z'}^2 - M_\Upsilon^2)}\right.$$
$$\left. + \frac{M_\Upsilon^2(3 - 4s_W^2)}{4c_W^2(M_Z^2 - M_\Upsilon^2)}\right). \qquad (4.2)$$

If we also neglect the last term from $Z - Z'$ interference, this expression agrees with Ref. [24]. The corresponding constraint on g_B is then

$$g_B < \sqrt{2}e\left(\sqrt{3|\Delta R_\Upsilon| + 1}\left|1 - \frac{M_{Z'}^2}{M_\Upsilon^2}\right| + \left(1 - \frac{M_{Z'}^2}{M_\Upsilon^2}\right)\right)^{1/2}, \qquad (4.3)$$

as shown in the low-mass gray-shaded region in Fig. 4. We have verified numerically that the precise constraint on g_B with finite final state masses and kinetic mixing from Eq. (3.11) gives a correction to Eq. (4.3) of less than 1%. Although our plot displays only masses above 5 GeV in Fig. 4, the constraint from $\Upsilon \to jj$ can be extended to lower $M_{Z'}$ values. For $M_{Z'} \sim 3$ GeV the constraint from J/ψ decay [31] is stringent, and below ~ 1 GeV additional experimental constraints become dominant [50].

In addition to limits from direct dijet resonance searches aimed at the Z'_B boson and indirect constraints from Z–Z'_B mixing and Υ decays, we also have constraints on the anomalons, which are required for self-consistency of the theory. One could introduce anomalons which replicate an entire generation of SM fermions but assign the new quarks $U(1)_B$ charge -1. The new fermions cancel the $[SU(2)_W]^2 \times U(1)_B$ and $[U(1)_Y]^2 \times U(1)_B$ anomalies, which are linear in the $U(1)_B$ charges, and also avoid generating new $U(1)_B$-gravity or $[U(1)_B]^3$ anomalies [51]. Phenomenologically, however, this solution is ruled out by the observed SM-like behavior of the 125 GeV Higgs boson, because the anomalons behave as a fourth generation of chiral fermions, which exhibit nondecoupling behavior in loop-induced Higgs processes. While additional states can, in principle, cancel these contributions [52], the nondecoupling nature of the anomalons in Higgs physics combined with the direct production probes for new quarks essentially excludes this solution. This discussion generalizes to any

solution where the anomalons are chiral under the SM gauge group.

A better option is to make the anomalons vector-like under the SM gauge group and chiral under $U(1)_B$. Because the only mixed anomalies from SM fields are $[SU(2)_W]^2U(1)_B$ and $[U(1)_Y]^2U(1)_B$, the new anomalons do not have to carry color [28–30,53–56], which significantly weakens their direct production rates at the LHC. Conversely, the anomalons do carry electric charge and, hence, mediate a nondecoupling diphoton partial width for the scalar associated with $U(1)_B$ breaking, which we will explore in a further publication.

An extra feature for hadronic Z'_B gauge bosons is the possible one-loop vanishing of $Z - Z'_B$ mixing at the anomalon mass scale, which amounts to a trace condition of all fermions charged under both groups, $\text{Tr}(z_B Y) = 0$, with z_B being the charges under $U(1)_B$. At energy scales below the anomalon masses, $Z - Z'_B$ mixing is reintroduced logarithmically.

Direct searches for the minimal model anomalons, in conjunction with a theoretical upper limit on the Yukawa couplings, rule out an additional region in the Z' mass-coupling plane [31]. Recall that the anomalon masses are generated by the Yukawa interactions (3.14) and the VEV $v_\phi = 2M_{Z'}/(3g_B)$. The perturbativity bound on the anomalon Yukawa couplings is roughly given by $y_L, y_E, y_N \lesssim 4\pi/3$, so that the anomalon masses satisfy $m_f \lesssim (8\pi/9)M_{Z'}/g_B$. Thus, an experimental lower limit on the anomalon masses translates into an upper limit on the gauge coupling $g_B < (8\pi/9)M_{Z'}/m_f$. The LEP constraint that the anomalons must be heavier than about 90 GeV rules out the blue-shaded region in Fig. 4.

Stronger lower limits on the anomalon masses could be imposed by searches at the LHC, but these are highly model dependent. For small mass splittings between the charged and neutral anomalons, their collider phenomenology is similar to charged and neutral Higgsino collider searches at the LHC [57–59], which are searched for using multilepton distributions and also metastable charged track signatures. For illustration, if an $m_f > 200$ GeV constraint is derived, then only the region below the straight dashed line in Fig. 4 is allowed by the perturbativity bound discussed above. It turns out, however, that there are regions in the parameter space where the mass limits on anomalons from the LHC are weaker than the one from LEP.

As an example, consider values for the Yukawa couplings in (3.14) that, after ϕ is replaced by its VEV, give the following anomalon mass terms: $m_f \bar{L}L + (m_f + \delta m_f)\bar{E}E + (m_f - \delta m_f)\bar{N}N$. Yukawa couplings of the anomalons to the Higgs doublet of the type $y_1 \bar{L}EH + y_2 \bar{N}LH$ lead through mass mixing to the decays of the charged anomalons to the neutral anomalons via off-shell W bosons, where the final state SM decay product is a charged pion (or a lepton and a neutrino, with a much smaller branching fraction). If $y_1, y_2 \approx \delta m_f / m_f$, then the decay width of a charged anomalon to a charged pion and a neutral anomalon is of the order of $(G_F^2/\pi)f_\pi^2 (\delta m)^3 \sqrt{1 - m_\pi^2/(\delta m)^2}$, where G_F is the Fermi decay constant and $f_\pi \approx 130.4$ MeV is the pion decay constant [60]. In our case, for $\delta m = 1$ GeV, the charged anomalon decay length is of the order of 10^{-2} mm in its rest frame and is prompt on collider length scales. Additional hadronic or leptonic decays become important as δm increases, which also increases the total decay width and shortens the charged anomalon lifetime. While Ref. [60] and subsequent collider phenomenology studies [61–66] and experimental searches [67,68] have focused on the metastable signature of charged winos and Higgsinos, the very difficult prompt decay signature into pions or charged leptons has also been emphasized [64].

Pair production of anomalons has the largest cross section when it is mediated by an off-shell W boson.

This cross section is $\sigma(L^+L^0) \approx 8$ pb for $m_f = 100$ GeV and $\delta m_f \ll m_f$ for $\sqrt{s} = 13$ TeV LHC [69] and is not large enough to allow events with highly boosted pions. Hence, the leading collider searches focus on the leptonic signatures, where the heavier neutral anomalon decays to the lighter neutral anomalon via an off-shell Z boson, giving a multilepton signature tested by ATLAS and CMS [57–59]. Such searches have significantly weakening sensitivity as δm becomes smaller than 5 GeV, where only the LEP exclusion limit survives when $\delta m \lesssim 1.5$ GeV. Moreover, the anomalon Drell-Yan cross section is about half of the Higgsino Drell-Yan cross section of 16.8 pb [70,71] for fully degenerate 100 GeV Higgsinos at the 13 TeV LHC, since we have only one $SU(2)$ doublet. Thus, the leptonic signals from the anomalons are also too weak to be seen by the LHC experiments thus far, and we adopt only the LEP constraint in our study.

As discussed in [72] and emphasized recently in [43,73–77], the Z boson can decay to Z' and a photon via a Wess-Zumino-Witten interaction from the nonzero anomaly induced by the nondecoupling effects of the anomalons as they become heavy. The full calculation of the partial width is found in Ref. [43], where the physics of the anomalons and the matching to the Wess-Zumino-Witten term is manifest.

From Ref. [43], the decay width of $Z \to Z'_B \gamma$ is

$$\Gamma(Z \to Z'_B \gamma) = \frac{\alpha_{\text{EM}} \alpha \alpha_B}{384\pi^2 c_W^2} \frac{m_Z'^2}{m_Z} \left(1 - \frac{m_{Z'}^4}{m_Z^4}\right) \left| - \sum_{f \in \text{SM}} T_3(f) Q_f^e \left[\frac{m_Z^2}{m_Z^2 - m_{Z'}^2}(B_0(m_Z^2, m_f) - B_0(m_{Z'}^2, m_f)) + 2m_f^2 C_0(m_f)\right] \right.$$

$$\left. + 3\left(\frac{m_Z^2}{m_Z^2 - m_{Z'}^2}(B_0(m_Z^2, M) - B_0(m_{Z'}^2, M)) + 2M^2 \frac{m_Z^2}{m_{Z'}^2} C_0(M)\right)\right|^2, \tag{4.4}$$

where $T_3(f) = +1$ for up-type quarks and -1 for down-type quarks, M is the mass of the anomalons and assumed to arise only from $U(1)_B$ breaking, and C_0 and B_0 are the usual Passarino-Veltman three-point and two-point scalar integrals, following the conventions of Package-X [78,79]:

$$B_0(m_V^2, m) \equiv B_0(m_V^2, m, m), \qquad C_0(m) \equiv C_0(0, m_Z^2, m_Z'^2, m, m, m). \tag{4.5}$$

We can construct an approximate expression for Eq. (4.4) by taking the first five SM quarks to be massless while the top quark and anomalons are taken to infinity. Note this expression is still valid only when the anomalon masses are solely generated from $U(1)_B$ breaking. The approximate partial width is then

$$\Gamma(Z \to Z'_B \gamma) \approx \frac{\alpha_{\text{EM}} \alpha \alpha_B}{384\pi^2 c_W^2} \frac{m_{Z'}^2}{m_Z} \left(1 - \frac{m_{Z'}^4}{m_Z^4}\right) \left|\frac{3m_Z^2}{m_{Z'}^2} - \frac{2}{3} - \frac{7}{3} \frac{m_Z^2}{m_Z^2 - m_{Z'}^2} \log\left(\frac{m_Z^2}{m_{Z'}^2}\right)\right|^2. \tag{4.6}$$

The pink region in Fig. 4 shows the limit calculated using Eq. (4.4) from the search of the L3 experiment for the exotic Z decay, $Z \to Z'\gamma$, $Z' \to jj$ [80], also taken from Ref. [43], where anomalon masses are fixed with Yukawa couplings $4\pi/3$ and arise solely from $U(1)_B$ breaking. The exotic decay constraint by L3 is competitive with the 35.9 fb^{-1} ISR γ search by CMS [14], although the indirect bound for charged anomalons still provides the dominant constraint [31].

V. CONCLUSIONS

We have analyzed the current state of the experimental collider searches for dijet resonances and compared them with the electroweak constraints on a Z' boson. Notably, the LHC experiments now provide the leading constraints not only at masses of several TeV, but also on electroweak scale dijet resonances, thanks to the advent of new trigger pathways and advanced data reconstruction methods.

In addition, the ATLAS and CMS experiments are also placing direct dijet bounds on resonances below 100 GeV, where legacy measurements from LEP experiments, constraints from Υ meson measurements, and indirect limits on charged anomalons compete for the strongest sensitivity. We have emphasized that, in gauged $U(1)_B$ models where the fermion sector obeys the orthogonality condition in Eq. (3.1), the kinetic mixing between SM and Z' gauge bosons is finite and only logarithmically sensitive to the anomalon masses. Moreover, the contribution of the anomalons to the exotic decay $Z \to Z'_B\gamma$ also follows nondecoupling behavior of chiral fermions, reducing the sensitivity on their mass scale. Thus, the coupling-mass plot, which is an insightful way of presenting the collider limits on dijet resonances, also allows a meaningful comparison with the low-energy data. Our summary of collider constraints, shown in Fig. 4, also includes the competing bounds from modifications to the properties of the Z and Υ due to the Z'_B, as well as the indirect limits from the Yukawa couplings of the anomalons.

We have also emphasized that, like the SM, the underlying chiral structure of the $U(1)_B$ symmetry is characterized by a single VEV, and, hence, the Z'_B and anomalon masses cannot be arbitrarily decoupled from each other without violating perturbative unitarity. In the coupling-versus-mass plane, the improving constraints continue to probe higher scales of $U(1)$ symmetry breaking, as evident from the diagonal lines corresponding to constant m_f anomalon masses in Fig. 4. The possible sensitivity improvements from collider searches for anomalons as well as signals of the symmetry-breaking sector (see, e.g., Ref. [81]) are left for future work.

APPENDIX: $Z'-Z$ MIXING

In this appendix, we compute the kinetic and mass mixings of the gauge eigenstate $Z'_{\rm ge}$ boson with the $Z_{\rm SM}$

boson, for general couplings (z^f) of $Z'_{\rm ge}$ to the fermions that satisfy the orthogonality relation $\mathrm{Tr}(Yz) = 0$, where Y is the hypercharge.

The one-loop amplitude for $Z'_{\rm ge} - Z_{\rm SM}$ mixing induced by fermions is given by $\epsilon_\mu \epsilon_\nu \mathcal{A}^{\mu\nu}$, where ϵ_μ and ϵ_ν are the polarization vectors of the two gauge bosons and

$$
\mathcal{A}^{\mu\nu} = i\frac{g_B g}{c_W}\mu^{4-D}\int\frac{d^D k}{(2\pi)^D}\sum_f\frac{N_f}{[(p+k)^2 - m_f^2](k^2 - m_f^2)}
$$
$$
\times \{m_f^2(g_L^f z_R^f + g_R^f z_L^f)g^{\mu\nu} + (g_L^f z_L^f + g_R^f z_R^f)
$$
$$
\times [p^\mu k^\nu + k^\mu p^\nu + 2k^\mu k^\nu - g^{\mu\nu}(p+k)\cdot k]\}. \quad (A1)
$$

Here, p is the 4-momentum of the $Z'_{\rm ge}$ and $Z_{\rm SM}$ bosons, and we used dimensional regularization with $D = 4 - \epsilon$ and a scale μ. The above sum is over the fermions f, which have a color factor N_f. Their right- and left-handed components (f_R and f_L) carry $Z'_{\rm ge}$ charges z_R^f and z_L^f, respectively, and also have couplings (g_R^f and g_L^f) to the $Z_{\rm SM}$ boson. After combining the denominators, we get

$$
\mathcal{A}^{\mu\nu} = i\frac{g_B g}{c_W}\int_0^1 dx \sum_f N_f \{m_f^2(g_L^f z_R^f + g_R^f z_L^f)g^{\mu\nu}I_0^f
$$
$$
+ (g_L^f z_L^f + g_R^f z_R^f)[g^{\mu\nu}I_1^f + x(1-x)
$$
$$
\times (g^{\mu\nu}p^2 - 2p^\mu p^\nu)I_0^f]\}, \quad (A2)
$$

where I_0^f and I_1^f are the following integrals:

$$
\{I_0^f, I_1^f\} = \mu^{4-D}\int\frac{d^D k}{(2\pi)^D}\frac{1}{[k^2 - m_f^2 + x(1-x)p^2]^2}
$$
$$
\times \left\{1, k^2\left(\frac{2}{D} - 1\right)\right\}. \quad (A3)
$$

The orthogonality relation $\mathrm{Tr}(Yz) = 0$ implies that the fermion charges satisfy

$$
\sum_f N_f(g_L^f z_L^f + g_R^f z_R^f) = 0. \quad (A4)
$$

Consequently, the apparent quadratic divergence of I_1^f in the $D = 4$ limit vanishes after the sum over fermions is performed. The usual ϵ expansion and the $\overline{\rm MS}$ scheme lead to the following expressions for the integrals:

$$
I_0^f = \frac{-i}{(4\pi)^2}\ln\left(\frac{m_f^2}{\mu^2} - x(1-x)\frac{p^2}{\mu^2} - i\epsilon_0\right),
$$
$$
I_1^f = -(m_f^2 - x(1-x)p^2)I_0^f, \quad (A5)
$$

where $i\epsilon_0$ is the prescription for the complex logarithm when $m_f^2 < x(1-x)p^2$.

The real part of the $Z'_{ge} - Z_{SM}$ mixing amplitude contains two pieces, as shown in Eq. (3.5): a kinetic mixing (with dimensionless coefficient κ_Z) and a mass mixing $\Delta M^2_{Z'Z}$ (the off-diagonal entry in the mass-squared matrix for the two gauge bosons). From Eq. (A2) and the second Eq. (A5) follows that

$$\kappa_Z = 2 \frac{g_B g}{c_W} \sum_f N_f \left(g_L^f z_L^f + g_R^f z_R^f\right) \operatorname{Re} i \int_0^1 dx x (1-x) I_0^f,$$

$$\Delta M^2_{Z'Z} = -\frac{g_B g}{c_W} \sum_f N_f m_f^2 \left(g_L^f - g_R^f\right)\left(z_L^f - z_R^f\right) \operatorname{Re} i \int_0^1 dx I_0^f.$$

$$(A6)$$

Integrating over x, we find

$$\int_0^1 dx x (1-x) I_0^f = \frac{-i}{6(4\pi)^2} \left[\ln\left(\frac{p^2}{\mu^2}\right) - \frac{5}{3} + \mathcal{F}(m_f^2/p^2) \right.$$
$$\left. + i\pi \mathcal{G}(m_f^2/p^2) \right].$$

$$(A7)$$

The functions introduced here are $\mathcal{G}(y) = \theta(1 - 4y) \times (1 + 2y)\sqrt{1 - 4y}$, where θ is the step function, and

$$\mathcal{F}(y) = \ln y - 4y + (1 + 2y)|4y - 1|^{1/2}$$
$$\times \begin{cases} \ln\left(\frac{1 + \sqrt{1 - 4y}}{2y} - 1\right) & \text{for } y \le \frac{1}{4}, \\ 2\arctan\left[(4y - 1)^{-1/2}\right] & \text{for } y > \frac{1}{4}. \end{cases}$$

$$(A8)$$

We emphasize that the sum over fermion loops removes not only the quadratic divergence from I_1^f, but also the logarithmically divergent part of each fermion loop, which is shown in (A7). Thus, the coefficient for kinetic mixing of any Z'_{ge} and Z_{SM} of 4-momentum p is *finite* and can be written as the following sum over the fermion loops:

$$\kappa_Z \simeq \frac{g_B g}{48\pi^2 c_W} \sum_f N_f \left(g_L^f z_L^f + g_R^f z_R^f\right) \mathcal{F}(m_f^2/p^2). \quad (A9)$$

This result is used in Sec. III. The expansion of the function $\mathcal{F}(y)$ for $y \ll 1/4$ is

$$\mathcal{F}(y) \simeq -6y + 6y^2 \ln y + O(y^2), \quad (A10)$$

while for $y \gg 1/4$

$$\mathcal{F}(y) \simeq \ln y + \frac{5}{3} - \frac{1}{5y} + O((4y)^{-2}). \quad (A11)$$

[1] T. Han, I. Lewis, and Z. Liu, Colored resonant signals at the LHC: Largest rate and simplest topology, J. High Energy Phys. 12 (2010) 085.

[2] R. M. Harris and K. Kousouris, Searches for dijet resonances at hadron colliders, Int. J. Mod. Phys. A **26**, 5005 (2011).

[3] B. A. Dobrescu and F. Yu, Coupling-mass mapping of dijet peak searches, Phys. Rev. D **88**, 035021 (2013); Phys. Rev. D **90**, 079901(E) (2014).

[4] M. Chala, F. Kahlhoefer, M. McCullough, G. Nardini, and K. Schmidt-Hoberg, Constraining dark sectors with monojets and dijets, J. High Energy Phys. 07 (2015) 089.

[5] C. Shimmin and D. Whiteson, Boosting low-mass hadronic resonances, Phys. Rev. D **94**, 055001 (2016).

[6] V. Khachatryan et al. (CMS Collaboration), Search for narrow resonances in dijet final states at $\sqrt{s} = 8$ TeV with the novel CMS technique of data scouting, Phys. Rev. Lett. **117**, 031802 (2016).

[7] A. M. Sirunyan et al. (CMS Collaboration), Search for low mass vector resonances decaying to quark-antiquark pairs in proton-proton collisions at $\sqrt{s} = 13$ TeV, Phys. Rev. Lett. **119**, 111802 (2017).

[8] A. M. Sirunyan et al. (CMS Collaboration), Search for low mass vector resonances decaying into quark-antiquark pairs in proton-proton collisions at $\sqrt{s} = 13$ TeV, J. High Energy Phys. 01 (2018) 097.

[9] M. Aaboud et al. (ATLAS Collaboration), Search for light resonances decaying to boosted quark pairs and produced in association with a photon or a jet in proton-proton collisions at $\sqrt{s} = 13$ TeV with the ATLAS detector, Phys. Lett. B **788**, 316 (2019).

[10] A. M. Sirunyan et al. (CMS Collaboration), Search for narrow resonances in the b-tagged dijet mass spectrum in proton-proton collisions at $\sqrt{s} = 8$ TeV, Phys. Rev. Lett. **120**, 201801 (2018).

[11] M. Aaboud et al. (ATLAS Collaboration), Search for low-mass dijet resonances using trigger-level jets with the ATLAS detector in pp collisions at $\sqrt{s} = 13$ TeV, Phys. Rev. Lett. **121**, 081801 (2018).

[12] M. Aaboud et al. (ATLAS Collaboration), Search for resonances in the mass distribution of jet pairs with one or two jets identified as b-jets in proton-proton collisions at $\sqrt{s} = 13$ TeV with the ATLAS detector, Phys. Rev. D **98**, 032016 (2018).

[13] M. Aaboud et al. (ATLAS Collaboration), Search for low-mass resonances decaying into two jets and produced in association with a photon using pp collisions at $\sqrt{s} = 13$ TeV with the ATLAS detector, Phys. Lett. B **795**, 56 (2019).

[14] A. M. Sirunyan *et al.* (CMS Collaboration), Search for low-mass quark-antiquark resonances produced in association with a photon at $\sqrt{s} = 13$ TeV, Phys. Rev. Lett. **123,** 231803 (2019).

[15] A. M. Sirunyan *et al.* (CMS Collaboration), Search for low mass vector resonances decaying into quark-antiquark pairs in proton-proton collisions at $\sqrt{s} = 13$ TeV, Phys. Rev. D **100,** 112007 (2019).

[16] A. M. Sirunyan *et al.* (CMS Collaboration), Search for dijet resonances using events with three jets in proton-proton collisions at $s = 13$ TeV, Phys. Lett. B **805,** 135448 (2020).

[17] G. Aad *et al.* (ATLAS Collaboration), Search for dijet resonances in events with an isolated charged lepton using $\sqrt{s} = 13$ TeV proton-proton collision data collected by the ATLAS detector, J. High Energy Phys. 06 (2020) 151.

[18] M. Aaboud *et al.* (ATLAS Collaboration), Search for new phenomena in dijet events using 37 fb^{-1} of pp collision data collected at $\sqrt{s} = 13$ TeV with the ATLAS detector, Phys. Rev. D **96,** 052004 (2017).

[19] A. M. Sirunyan *et al.* (CMS Collaboration), Search for narrow and broad dijet resonances in proton-proton collisions at $\sqrt{s} = 13$ TeV and constraints on dark matter mediators and other new particles, J. High Energy Phys. 08 (2018) 130.

[20] CMS Collaboration, Searches for dijet resonances in pp collisions at $\sqrt{s} = 13$ TeV using the 2016 and 2017 datasets, Report No. PAS-EXO-17-026, 2018, https://inspirehep.net/record/1693731.

[21] G. Aad *et al.* (ATLAS Collaboration), Search for new resonances in mass distributions of jet pairs using 139 fb^{-1} of pp collisions at $\sqrt{s} = 13$ TeV with the ATLAS detector, J. High Energy Phys. 03 (2020) 145.

[22] A. M. Sirunyan *et al.* (CMS Collaboration), Search for high mass dijet resonances with a new background prediction method in proton-proton collisions at $\sqrt{s} = 13$ TeV, J. High Energy Phys. 05 (2020) 033.

[23] A. Pais, Remark on baryon conservation, Phys. Rev. D **8,** 1844 (1973).

[24] C. D. Carone and H. Murayama, Possible light U(1) gauge boson coupled to baryon number, Phys. Rev. Lett. **74,** 3122 (1995).

[25] D. C. Bailey and S. Davidson, Is there a vector boson coupling to baryon number?, Phys. Lett. B **348,** 185 (1995).

[26] C. D. Carone and H. Murayama, Realistic models with a light U(1) gauge boson coupled to baryon number, Phys. Rev. D **52,** 484 (1995).

[27] A. Aranda and C. D. Carone, Limits on a light leptophobic gauge boson, Phys. Lett. B **443,** 352 (1998).

[28] P. Fileviez Perez and M. B. Wise, Breaking local baryon and lepton number at the TeV scale, J. High Energy Phys. 08 (2011) 068.

[29] M. Duerr, P. Fileviez Perez, and M. B. Wise, Gauge theory for baryon and lepton numbers with leptoquarks, Phys. Rev. Lett. **110,** 231801 (2013).

[30] P. Fileviez Perez, S. Ohmer, and H. H. Patel, Minimal theory for lepto-baryons, Phys. Lett. B **735,** 283 (2014).

[31] B. A. Dobrescu and C. Frugiuele, Hidden GeV-scale interactions of quarks, Phys. Rev. Lett. **113,** 061801 (2014).

[32] B. A. Dobrescu, Leptophobic boson signals with leptons, jets and missing energy, arXiv:1506.04435.

[33] B. A. Dobrescu, P. J. Fox, and J. Kearney, Higgs-photon resonances, Eur. Phys. J. C **77,** 704 (2017).

[34] J. Y. Araz, G. Corcella, M. Frank, and B. Fuks, Loopholes in Z' searches at the LHC: Exploring supersymmetric and leptophobic scenarios, J. High Energy Phys. 02 (2018) 092.

[35] J. Alwall, R. Frederix, S. Frixione, V. Hirschi, F. Maltoni, O. Mattelaer, H.-S. Shao, T. Stelzer, P. Torrielli, and M. Zaro, The automated computation of tree-level and next-to-leading order differential cross sections, and their matching to parton shower simulations, J. High Energy Phys. 07 (2014) 079.

[36] A. Alloul, N. D. Christensen, C. Degrande, C. Duhr, and B. Fuks, FeynRules 2.0—A complete toolbox for tree-level phenomenology, Comput. Phys. Commun. **185,** 2250 (2014).

[37] T. Hahn, Generating Feynman diagrams and amplitudes with FeynArts 3, Comput. Phys. Commun. **140,** 418 (2001).

[38] R. D. Ball *et al.* (NNPDF Collaboration), Parton distributions from high-precision collider data, Eur. Phys. J. C **77,** 663 (2017).

[39] J. Dolen, P. Harris, S. Marzani, S. Rappoccio, and N. Tran, Thinking outside the ROCs: Designing decorrelated taggers (DDT) for jet substructure, J. High Energy Phys. 05 (2016) 156; C. Shimmin, P. Sadowski, P. Baldi, E. Weik, D. Whiteson, E. Goul, and A. Sogaard, Decorrelated jet substructure tagging using adversarial neural networks, Phys. Rev. D **96,** 074034 (2017).

[40] G. Aad *et al.* (ATLAS Collaboration), Search for dijet resonances in events with an isolated charged lepton using $\sqrt{s} = 13$ TeV proton-proton collision data collected by the ATLAS detector, J. High Energy Phys. 06 (2020) 151.

[41] F. Yu, Di-jet resonances at future hadron colliders: A Snowmass whitepaper, arXiv:1308.1077.

[42] M. L. Graesser, I. M. Shoemaker, and L. Vecchi, A dark force for baryons, arXiv:1107.2666.

[43] L. Michaels and F. Yu, Probing new U(1) gauge symmetries via exotic $Z \rightarrow Z'\gamma$ decays, J. High Energy Phys. 03 (2021) 120.

[44] J. Liu, X. P. Wang, and F. Yu, A tale of two portals: Testing light, hidden new physics at future e^+e^- colliders, J. High Energy Phys. 06 (2017) 077.

[45] R. L. Workman *et al.* (Particle Data Group), Review of particle physics, Prog. Theor. Exp. Phys. **2022,** 083C01 (2022).

[46] A. Hook, E. Izaguirre, and J. G. Wacker, Model independent bounds on kinetic mixing, Adv. High Energy Phys. **2011,** 859762 (2011).

[47] H. Albrecht *et al.* (ARGUS Collaboration), An upper limit for two jet production in direct $\Upsilon(1s)$ decays, Z. Phys. C **31,** 181 (1986).

[48] T. Appelquist and H. D. Politzer, Orthocharmonium and e^+e^- annihilation, Phys. Rev. Lett. **34,** 43 (1975).

[49] E. L. Berger and D. L. Jones, Inelastic photoproduction of J/ψ and Υ by gluons, Phys. Rev. D **23,** 1521 (1981).

[50] S. Tulin, New weakly-coupled forces hidden in low-energy QCD, Phys. Rev. D **89,** 114008 (2014).

[51] P. Fileviez Perez and M. B. Wise, Baryon and lepton number as local gauge symmetries, Phys. Rev. D **82,** 011901 (2010); Phys. Rev. D **82,** 079901(E) (2010).

[52] K. Kumar, R. Vega-Morales, and F. Yu, Effects from new colored states and the Higgs portal on gluon fusion and Higgs decays, Phys. Rev. D **86**, 113002 (2012); Phys. Rev. D **87**, 119903(E) (2013).

[53] M. Carena, A. Daleo, B. A. Dobrescu, and T. M. P. Tait, Z' gauge bosons at the Tevatron, Phys. Rev. D **70**, 093009 (2004).

[54] M. Duerr and P. Fileviez Perez, Baryonic dark matter, Phys. Lett. B **732**, 101 (2014).

[55] J. M. Arnold, P. Fileviez Perez, B. Fornal, and S. Spinner, B and L at the supersymmetry scale, dark matter, and R-parity violation, Phys. Rev. D **88**, 115009 (2013).

[56] S. Ohmer and H. H. Patel, Leptobaryons as Majorana dark matter, Phys. Rev. D **92**, 055020 (2015).

[57] G. Aad *et al.* (ATLAS Collaboration), Searches for electroweak production of supersymmetric particles with compressed mass spectra in $\sqrt{s} = 13$ TeV pp collisions with the ATLAS detector, Phys. Rev. D **101**, 052005 (2020).

[58] CMS Collaboration, Combined search for electroweak production of winos, binos, higgsinos, and sleptons in proton-proton collisions at $\sqrt{s} = 13$ TeV, Report No. CMS-PAS-SUS-21-008, https://inspirehep.net/literature/2646012.

[59] ATLAS Collaboration, Run 2 results of searches for charginos and neutralinos at the ATLAS experiment using a statistical combination, Report No. ATLAS-CONF-2023-046, https://inspirehep.net/literature/2698573.

[60] S. D. Thomas and J. D. Wells, Phenomenology of massive vectorlike doublet leptons, Phys. Rev. Lett. **81**, 34 (1998).

[61] A. Arvanitaki, N. Craig, S. Dimopoulos, and G. Villadoro, Mini-split, J. High Energy Phys. 02 (2013) 126.

[62] L. J. Hall, Y. Nomura, and S. Shirai, Spread supersymmetry with wino LSP: Gluino and dark matter signals, J. High Energy Phys. 01 (2013) 036.

[63] N. E. Bomark, A. Kvellestad, S. Lola, P. Osland, and A. R. Raklev, Long lived charginos in natural SUSY?, J. High Energy Phys. 05 (2014) 007.

[64] Z. Han, G. D. Kribs, A. Martin, and A. Menon, Hunting quasidegenerate higgsinos, Phys. Rev. D **89**, 075007 (2014).

[65] N. Nagata and S. Shirai, Higgsino dark matter in high-scale supersymmetry, J. High Energy Phys. 01 (2015) 029.

[66] M. Saito, R. Sawada, K. Terashi, and S. Asai, Discovery reach for wino and Higgsino dark matter with a disappearing track signature at a 100 TeV pp collider, Eur. Phys. J. C **79**, 469 (2019).

[67] G. Aad *et al.* (ATLAS Collaboration), Search for metastable heavy charged particles with large ionisation energy loss in pp collisions at $\sqrt{s} = 8$ TeV using the ATLAS experiment, Eur. Phys. J. C **75**, 407 (2015).

[68] M. Aaboud *et al.* (ATLAS Collaboration), Search for metastable heavy charged particles with large ionization energy loss in pp collisions at $\sqrt{s} = 13$ TeV using the ATLAS experiment, Phys. Rev. D **93**, 112015 (2016).

[69] N. Kumar and S. P. Martin, Vectorlike leptons at the Large Hadron Collider, Phys. Rev. D **92**, 115018 (2015).

[70] B. Fuks, M. Klasen, D. R. Lamprea, and M. Rothering, Gaugino production in proton-proton collisions at a center-of-mass energy of 8 TeV, J. High Energy Phys. 10 (2012) 081.

[71] B. Fuks, M. Klasen, D. R. Lamprea, and M. Rothering, Precision predictions for electroweak superpartner production at hadron colliders with Resummino, Eur. Phys. J. C **73**, 2480 (2013).

[72] J. Preskill, Gauge anomalies in an effective field theory, Ann. Phys. (N.Y.) **210**, 323 (1991).

[73] Y. Cui and F. D'Eramo, Surprises from complete vector portal theories: New insights into the dark sector and its interplay with Higgs physics, Phys. Rev. D **96**, 095006 (2017).

[74] J. A. Dror, R. Lasenby, and M. Pospelov, New constraints on light vectors coupled to anomalous currents, Phys. Rev. Lett. **119**, 141803 (2017).

[75] A. Ismail, A. Katz, and D. Racco, On dark matter interactions with the Standard Model through an anomalous Z', J. High Energy Phys. 10 (2017) 165.

[76] J. A. Dror, R. Lasenby, and M. Pospelov, Dark forces coupled to nonconserved currents, Phys. Rev. D **96**, 075036 (2017).

[77] A. Ismail and A. Katz, Anomalous Z' and diboson resonances at the LHC, J. High Energy Phys. 04 (2018) 122.

[78] H. H. Patel, Package-X: A *Mathematica* package for the analytic calculation of one-loop integrals, Comput. Phys. Commun. **197**, 276 (2015); Package-X 2.0: A *Mathematica* package for the analytic calculation of one-loop integrals, Comput. Phys. Commun. **218**, 66 (2017).

[79] G. Passarino and M. J. G. Veltman, One loop corrections for e^+e^- annihilation into $\mu^+\mu^-$ in the Weinberg model, Nucl. Phys. **B160**, 151 (1979).

[80] O. Adriani *et al.* (L3 Collaboration), Isolated hard photon emission in hadronic Z^0 decays, Phys. Lett. B **292**, 472 (1992).

[81] M. Duerr, P. F. Perez, and J. Smirnov, Baryonic Higgs at the LHC, J. High Energy Phys. 09 (2017) 093.